Dalton Transactions

PAPER

View Article Online
View Journal | View Issue



Cite this: *Dalton Trans.*, 2015, **44**, 15576

# $K_3LaTe_2O_9$: a new alkali-rare earth tellurate with face-sharing $TeO_6$ octahedra†

Xinyuan Zhang,[a,b] Jiyong Yao,[a] Xingxing Jiang,[a,b] Ying Fu,[a,b] Zheshuai Lin,[a] Guochun Zhang*[a] and Yicheng Wu[a]

Received 14th June 2015,
Accepted 23rd July 2015

DOI: 10.1039/c5dt02255j

www.rsc.org/dalton

A new quaternary alkali-lanthanide metal tellurate $K_3LaTe_2O_9$ has been synthesized by a conventional high-temperature solid state method, and single crystals have been grown by spontaneous crystallization. $K_3LaTe_2O_9$ crystallizes in the hexagonal space group $P6_3/mmc$, with $a = b = 6.0589(9)$ Å, $c = 15.024(3)$ Å, and $Z = 2$. In the structure, $[Te_2O_9]^{6-}$ contains rare face-sharing $TeO_6$ polyhedra, which are connected by $LaO_6$ octahedra forming a three-dimensional framework structure. Furthermore, its properties are investigated by UV-vis-NIR diffuse reflectance spectroscopy, Raman and IR spectroscopy, thermal analysis, variable-temperature X-ray powder diffraction, and first-principles calculations.

## Introduction

Tellurates have attracted much attention because of their rich structural chemistry and interesting physical properties, such as nonlinear optical (NLO) properties, ferroelectric properties, magnetic properties, *etc.*[1–4] Generally, the Te stereochemistry plays an important role in determining the overall atomic and electronic structures and physical properties.[5–8] For instance, in $BaMTe^{IV}Te^{VI}O_7$ (M = $Mg^{2+}$ or $Zn^{2+}$), $Te^{VI}O_6$ octahedra link with asymmetric $Te^{IV}O_4$ polyhedra to form a continuous layer with polar symmetry, leading to a moderate second harmonic generating capability.[1] $A_2CoTeO_6$ perovskites (A = Cd, Ca, Sr, Pb, and Ba) are antiferromagnetic at low temperatures, and the unique decrease in antiferromagnetic interactions shows that $Te^{6+}$ cations affect the electronic and the magnetic structure in the compounds, which is not observed in $A_2^{2+}CoM^{6+}O_6$ with other similar ionic sizes of $M^{6+}$.[2]

Until now, quaternary alkali-rare earth metal tellurate compounds have seldom been reported besides polycrystalline $Eu^{3+}$-doped $Li_3Y_3Te_2O_{12}$.[9] Since La has the $d^0$ electronic configuration, which can induce distortion of coordination polyhedra through a second-order Jahn–Teller effect[10] leading to interesting structures and properties, many efforts were made to synthesize new A/La/TeO compounds. For example, $A_2(BB')O_6$ perovskite compounds $MLaMgTeO_6$ (M = Na, K) show layer-like ordering of alkali and $La^{3+}$ ions in A sites, with strong distortion of $MgO_6$ and $TeO_6$ octahedra.[11]

In order to search for novel structures or new functional materials, we investigated further the alkali-rare earth tellurate systems, which led us to find $K_3LaTe_2O_9$, a rare quaternary alkali-lanthanide tellurate, with only the second refined structure after $Ba_3Te_2O_9$ [11,12] in which $TeO_6$ octahedra share faces rather than edges or corners. In this work, we present the growth, structure, optical and thermal properties of $K_3LaTe_2O_9$ crystals.

## Experimental section

### Synthesis and growth

Polycrystalline samples of $K_3LaTe_2O_9$ were prepared by solid-state reaction. The initial reactants were $K_2CO_3$, $La_2O_3$, and $H_6TeO_6$ (all analytically pure). Before weighing, $La_2O_3$ was preheated at 600 °C for 12 h to remove $H_2O$. A mixture of $K_2CO_3$, $La_2O_3$, and $H_6TeO_6$ in a molar ratio of 3 : 1 : 4 was ground and preheated in an $Al_2O_3$ crucible at 400 °C in air for 10 h to decompose the carbonate and eliminate the water. The products were cooled to room temperature and ground. Then the products were heated to 650 °C and held for three days with several intermediate grindings until single-phase powders were obtained.

X-ray powder diffraction analysis of the polycrystalline samples was performed at room temperature using an automated Bruker D8 X-ray diffractometer equipped with a diffracted monochromator set for Cu Kα ($\lambda$ = 1.5418 Å) radiation. A scanning step width of 0.02° and a scanning rate of 0.1 s per step were applied to record the pattern in the 2$\theta$ range of

[a]*Beijing Center for Crystal Research and Development, Key Laboratory of Functional Crystals and Laser Technology, Technical Institute of Physics and Chemistry, Chinese Academy of Sciences, Beijing 100190, P. R. China. E-mail: gczhang@mail.ipc.ac.cn*
[b]*University of Chinese Academy of Sciences, Beijing 100049, P. R. China*
†CCDC 1406510. For crystallographic data in CIF or other electronic format see DOI: 10.1039/c5dt02255j

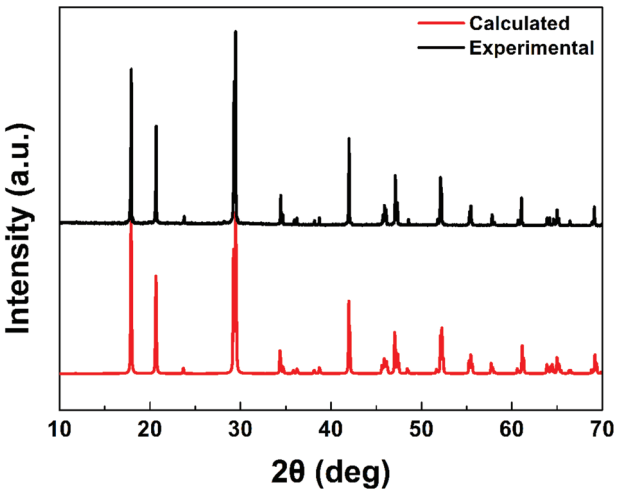


Fig. 1 Calculated and experimental X-ray diffraction patterns of $K_3LaTe_2O_9$.

10–70°. The XRD pattern of $K_3LaTe_2O_9$ powder was in good agreement with the calculated pattern on the basis of the single crystal crystallographic data of $K_3LaTe_2O_9$ (Fig. 1).

Single crystals of $K_3LaTe_2O_9$ were grown by spontaneous crystallization. A mixture of $K_2CO_3$, $La_2O_3$, and $H_6TeO_6$ in a molar ratio of 3 : 1 : 6 was ground in an agate mortar and melted in a platinum crucible in several batches. The crucible was placed in a programmable temperature furnace, heated to 650 °C in air, and held for 10 h, then slowly cooled to 200 °C at a rate of 3–4 °C $h^{-1}$ followed by rapid cooling to room temperature. The product consisted of colorless crystals, which were manually selected for structure characterization. EDX analysis was carried out on a Hitachi S-4800 SEM, which showed that the approximate molar ratio of K, La, and Te is 3 : 1 : 2. ICP-AES was carried out on an IRIS Intrepid II XSP, which showed that the molar ratio of K, La, and Te is 3.2 : 1 : 2.3.

### Structure determination

Single-crystal X-ray diffraction data at 153 K were collected on a Rigaku AFC10 diffractometer (Mo Kα, $\lambda$ = 0.71073 Å) equipped with a Saturn CCD detector. Crystal decay was monitored by re-collecting 50 initial frames at the end of data collection. The collection of the intensity data, cell refinement, and data reduction were carried out with the program CrystalClear.[13] Face-indexed absorption corrections were performed numerically by using the program XPREP.[14]

The structure was solved with the direct methods program SHELXS and refined with the least-squares program SHELXL of the SHELXTL.PC suite of programs.[14] The final refinement included anisotropic displacement parameters and a secondary extinction correction. The program STRUCTURE TIDY[15] was then employed to standardize the atomic coordinates. Additional details and structural data are given in Tables 1–3, and further information can be found in the ESI.†

Table 1 Crystal data and structure refinements for $K_3LaTe_2O_9$

| | $K_3LaTe_2O_9$ |
|---|---|
| $F_w$ | 655.41 |
| Crystal system | Hexagonal |
| Space group | $P6_3/mmc$ |
| $a$ (Å) | 6.0589(9) |
| $c$ (Å) | 15.024(3) |
| $V$ (Å$^3$) | 477.6(1) |
| $Z$ | 2 |
| $T$ (K) | 153 |
| $\Lambda$ (Å) | 0.71073 |
| $\rho_c$ (g cm$^{-3}$) | 4.557 |
| $\mu$ (cm$^{-1}$) | 11.792 |
| $R_{int}$ | 0.0377 |
| $R(F)^a$ | 0.0227 |
| $R_w(F_o^2)^b$ | 0.0465 |

$^a$ $R(F) = \sum||F_o| - |F_c||/\sum|F_o|$ for $F_o^2 > 2\sigma(F_o^2)$. $^b$ $R_w(F_o^2) = \{\sum[w(F_o^2 - F_c^2)^2]/\sum wF_o^4\}^{1/2}$ for all data. $w^{-1} = \sigma^2(F_o^2) + (zP)^2$, where $P = (\mathrm{Max}(F_o^2, 0) + 2F_c^2)/3$; $z = 0.02$.

Table 2 Selected bond lengths (Å) and bond angles (°) for $K_3LaTe_2O_9$

| | | | |
|---|---|---|---|
| K1–O2 × 7 | 3.000(3) | K2–O2 × 3 | 3.0505(18) |
| K1–O1 × 6 | 3.0454(6) | La1–O2 × 7 | 2.358(3) |
| K1–O1 | 3.0505(18) | Te1–O2 × 3 | 1.860(3) |
| K2–O1 × 4 | 2.875(3) | Te1–O1 × 4 | 2.016(3) |
| K2–O2 × 5 | 3.0504(6) | O2–Te1–O2 × 3 | 97.52(12) |
| O2–La1–O2 × 6 | 87.49(10) | O2–Te1–O1 × 6 | 92.18(9) |
| O2–La1–O2 × 6 | 92.51(10) | O2–Te1–O1 × 3 | 165.24(12) |
| O2–La1–O2vi × 3 | 180.0(1) | O1–Te1–O1 × 3 | 76.29(12) |
| Te1–O1–Te1 | 89.00(15) | Te1–O2–La1 | 172.71(16) |

Table 3 Atomic coordinates, equivalent isotropic displacement parameters (Å$^2$), and calculated bond valence sum (BVS) for $K_3LaTe_2O_9$

| Atom | Wyck. | Site | $x/a$ | $y/b$ | $z/c$ | $U_{eq}$ $^a$ (Å$^2$) | BVS |
|---|---|---|---|---|---|---|---|
| K1 | 2b | -6m2 | 0 | 0 | 3/4 | 0.0086(4) | 1.086 |
| K2 | 4f | 3m. | 1/3 | 2/3 | 0.61656(11) | 0.0122(3) | 0.909 |
| La1 | 2a | -3m. | 0 | 0 | 1/2 | 0.00297(16) | 3.414 |
| Te1 | 4f | 3m. | −1/3 | 1/3 | 0.65593(3) | 0.00287(15) | 5.784 |
| O1 | 6h | mm2 | −0.0592(7) | 0.4704(4) | 3/4 | 0.0049(7) | 1.964 |
| O2 | 12k | .m. | −0.6412(5) | 0.1794(2) | 0.5945(2) | 0.0088(6) | 1.916 |

$^a$ $U_{eq}$ is defined as one-third of the trace of the orthogonalized $U_{ij}$ tensor.

### First-principles calculations

The first-principles studies on the electronic density difference and Mulliken atomic/bond populations[16] were performed by the plane-wave pseudopotential method[17] implemented in the CASTEP package[18] based on density functional theory (DFT).[19] The functional[20] developed by Ceperley, Alder, Perdew and Zunger (CA-PZ) in local density approximation (LDA) form was adopted to search the minimum of the electron energy. The optimized norm-conserving pseudopotentials[21] in Kleinman–Bylander form[22] allow us to use a small plane basis set without compromising the accuracy required by the calculation. The kinetic energy cutoff of 900 eV and Monkhorst–Pack *k*-point mesh spanning less than 0.03 $Å^{-1}$ in the Brillouin zone were chosen.[23]

### Spectroscopic characterization

A Cary 5000 UV-vis-NIR spectrophotometer with a diffuse reflectance accessory was used to record the diffuse reflectance spectrum of $K_3LaTe_2O_9$ in the range of 200–2500 nm. The mid-infrared spectrum in a range from 400 to 1200 $cm^{-1}$ at room temperature was obtained using a Bio-Rad FTS-60 FTIR spectrometer with a resolution of 1 $cm^{-1}$. The Raman pattern from 100 to 1200 $cm^{-1}$ at room temperature was recorded on Via-Reflex equipped with a 532 nm solid state laser.

### Thermal analysis

A Labsys™ TG-DTA16 (SETARAM) thermal analyzer was used to investigate the thermal properties by differential scanning calorimetric (DSC) analysis. About 10 mg $K_3LaTe_2O_9$ samples were placed in an $Al_2O_3$ crucible, heated at a rate of 10 °C $min^{-1}$ from room temperature to 900 °C and then cooled to room temperature at the same rate. The thermal gravimetric analysis (TGA) in nitrogen was performed on a Perkin-Elmer Diamond TG/DTA spectrometer, and the heating rate was about 10 °C $min^{-1}$.

### Variable-temperature X-ray powder diffraction (VT-XRD)

The variable-temperature X-ray powder diffraction was recorded on a Bruker D8-discover X-ray diffractometer equipped with a diffracted monochromator set for Cu Kα ($\lambda$ = 1.5418 Å). Patterns at high temperature (298–1123 K) were separately recorded with a scanning step width of 0.01°. The high-temperature conditions were obtained using an Anton Paar HTK 1200N high-temperature oven.

## Results and discussion

### Crystal structure

As seen in Fig. 2, the $K_3LaTe_2O_9$ compound crystallizes in the centrosymmetric hexagonal space group $P6_3/mmc$. There are two crystallographically independent K atoms, one independent La atom, one independent Te atom, and two independent O atoms in the symmetry unit. K1, K2, La1, Te1, O1, and O2 atoms are in the Wyckoff sites 2b, 4f, 2a, 4f, 6h, and 12k, respectively. The occupancy of all sites is 100%. The oxidation state of 1+, 3+, 6+, and 2− can be assigned to K, La, Te, and O atoms, respectively.

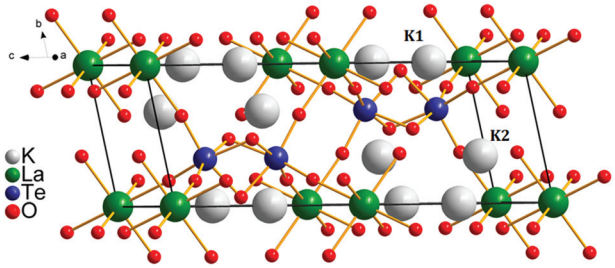


Fig. 2 Crystal structure of $K_3LaTe_2O_9$.

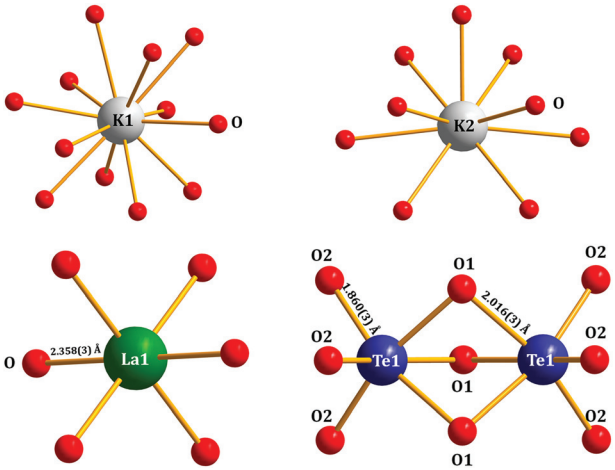


Fig. 3 Coordination environments of the cations in $K_3LaTe_2O_9$.

The coordination environments of the cations in $K_3LaTe_2O_9$ are shown in Fig. 3. In its structure, Te1 atoms are coordinated to six O atoms to form distorted octahedra. Te–O bond lengths are respectively 1.860(3) Å for O(2) atoms, which share corners with $LaO_6$ octahedra, and 2.016(3) Å for O(1) atoms, which form the face shared by two $TeO_6$ octahedra, similar to that of $Ag_2Te_2O_6$ (1.8635 Å to 2.0420 Å) and $Ba_3Te_2O_9$ (1.8455 Å to 1.9925 Å).[12,24] The Te1–O–Te1 angles in $[Te_2O_9]^{6-}$ anions are almost 89.00(15)°, resembling $Ba_3Te_2O_9$ (89.720°) in a similar coordination environment. Since each $TeO_6$ is linked to only one other, these octahedra form isolated face-sharing dimeric anions, $[Te_2O_9]^{6-}$. Meanwhile, La atoms are linked to six O atoms in regular octahedra with the La–O bond lengths of 2.358(3) Å. The La–O–Te angles are 172.71(16)°, comparable to those in the similar coordination environment of (Fe)2a–O2–(Fe/Te)4f in $Ba_3Fe_2TeO_9$ (175.3(1)°).[3] K1 atoms are surrounded by twelve O atoms to form distorted cuboctahedra with K–O bond lengths from 3.000(3) Å to 3.0505(18) Å, and K2 atoms are surrounded by nine O atoms to form distorted octahedra with K–O bond lengths from 2.875(3) Å to 3.051(4) Å. The terminal oxygen atoms in $[Te_2O_9]^{6-}$ anions are linked by sharing

 

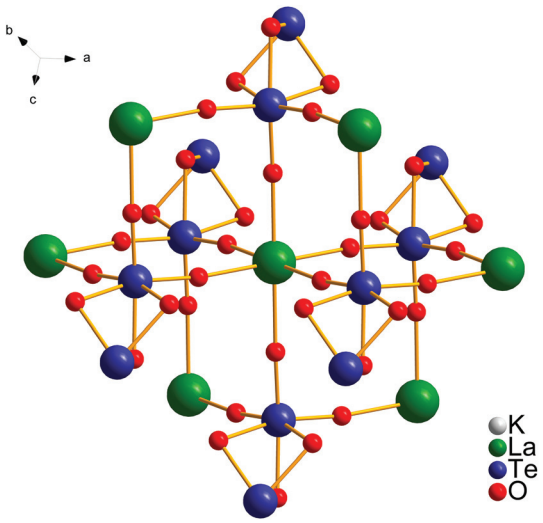


Fig. 4 Framework diagram of $K_3LaTe_2O_9$.

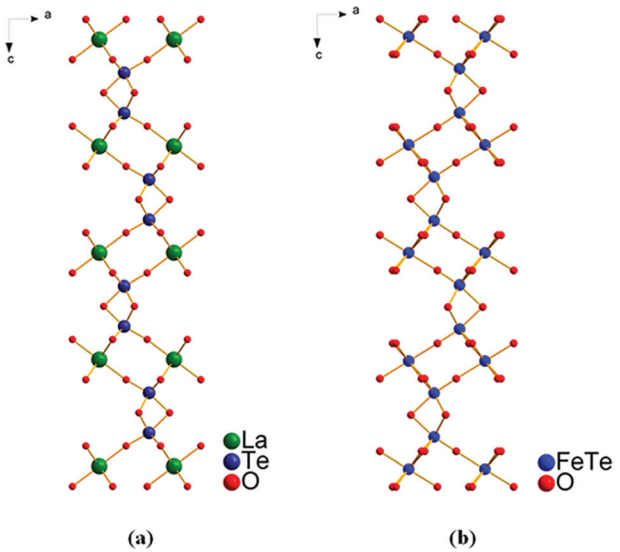


Fig. 5 $Te_2O_9$ groups and $FeTeO_9$ groups in $K_3LaTe_2O_9$ (a) and $Ba_3Fe_2TeO_9$ (b).

corners with the $LaO_6$ octahedron and build a three-dimensional framework structure. $K^+$ cations occupied the interstices surrounded by Te–O polyhedra and La–O polyhedra, as seen in Fig. 4.

According to Pauling's third and fourth rules, repulsion between high-charge cations means that polyhedra containing them are most stable if they share corners, less stable if they share edges and even less so if they share faces.[25,26] Thus, the corner-sharing pattern is the most common way to connect polyhedra in inorganic compounds, such as borates, silicates, phosphates, and tellurates.[27–30] The edge- or face-sharing patterns are rarely found in the above compounds except under extreme conditions, for instance, $Dy_4B_6O_{15}$ with edge-sharing $BO_4$ tetrahedra was synthesized under high-pressure (8 GPa) and high-temperature (1000 °C).[31] So far as we know, in tellurates, Te atoms commonly coordinate with six oxygen atoms forming $TeO_6$ octahedra, and $TeO_6$ octahedra are usually isolated or connected by sharing corners forming a three-dimensional framework, hence tellurates with face sharing $TeO_6$ octahedra are very rare. Only $Ba_3Te_2O_9$ and $Ba_3Fe_2TeO_9$ exhibit face-sharing $TeO_6$ octahedral structures and $Ba_3Fe_2TeO_9$ shows face-sharing between Fe and Te, not totally two Te cations, while $K_3LaTe_2O_9$ is the first alkali-rare earth metal quaternary tellurate with face-sharing $TeO_6$ octahedral structures. Therefore, the discovery of $K_3LaTe_2O_9$ shows the potential of the lanthanide tellurates for displaying new types of crystal structures.

As mentioned above, the structure of $K_3LaTe_2O_9$ is similar to that of $Ba_3Te_2O_9$ and $Ba_3Fe_2TeO_9$.[3,12] The structure of $Ba_3Te_2O_9$ was determined by neutron power diffraction. It occurs in the space group $P6_3/mmc$ with unit cell parameters ($a$ = 5.8603 Å, $c$ = 14.3037 Å). Ba1, Ba2, Te1, O1, and O2 are in the Wyckoff sites 2d, 4f, 4e, 6h, and 12k, respectively, with 100% occupation of all atoms, and $[Te_2O_9]^{6-}$ anions are separated by $Ba^{2+}$, which are obviously different from the distributions of the cations in $K_3LaTe_2O_9$. As to $Ba_3Fe_2TeO_9$, the structure was solved and refined on the basis of neutron power diffraction data, which also belongs to the space group $P6_3/mmc$ with unit cell parameters ($a$ = 5.767 Å, $c$ = 14.1998 Å). $Ba_3Fe_2TeO_9$ is actually isostructural with $K_3LaTe_2O_9$, with K1, K2, La, and Te in the latter compound corresponding to Ba1, Ba2, M1 (M = $Fe_{0.85}Te_{0.15}$) and M2 (M = $Fe_{0.57}Te_{0.43}$) in the former. Besides, $FeTeO_9$ groups in $Ba_3Fe_2TeO_9$ and $Te_2O_9$ groups in $K_3LaTe_2O_9$ are centrosymmetrical structures with mirror planes (Fig. 5).

## First-principles calculations

The first-principles studies were performed to further investigate the mechanism of the structural stability of the face-sharing $[Te_2O_9]^{6-}$ anion. As we know, vibrations in the low frequency region are more likely to break up because they would shift to an imaginary frequency region under external environmental disturbance.[32] In the $K_3LaTe_2O_9$ structure, related Te–O Raman spectral calculation results in a low frequency around 200 $cm^{-1}$ correspond to the vibration along the same direction of the $[Te_2O_9]$ group (as seen in Fig. 10(a)). This kind of vibration would not cause the break of the face-sharing $[Te_2O_9]$ group, thus the face-sharing $[Te_2O_9]^{6-}$ anion is stable to some extent. Fig. 10(b) exhibits the electronic density difference in the face-sharing $[Te_2O_9]$ groups, which shows a different charge redistribution among the face-sharing O(1) and corner-sharing O(2). In detail, O(2) atoms obtain more electronic charges from the neighboring Te atoms, which indicates migration of electronic charges from Te–O(1) to Te–O(2) bonds due to the modification of the chemical environment around the oxygen atoms as they are changed from face-sharing to corner-sharing. More quantitative results from the Mulliken analysis reveal that Te–O(1) and Te–O(2) Mulliken populations

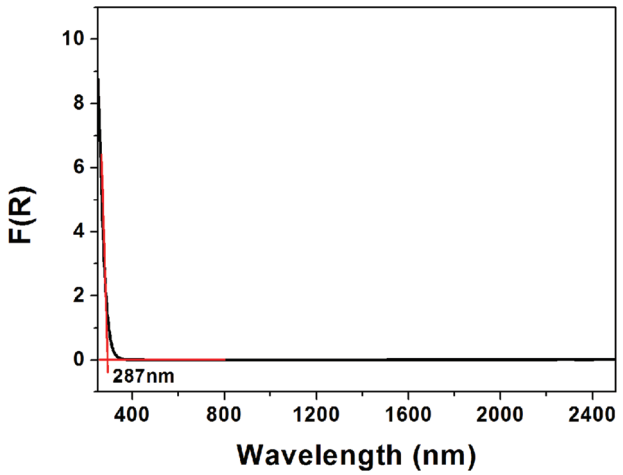


Fig. 6 Diffuse reflectance spectrum of $K_3LaTe_2O_9$.

are 0.44 and 0.62, respectively. This implies that the corner-sharing oxygen atoms are more stable than the face-sharing oxygen atoms, consistent with the Pauling's second rule (*i.e.*, the oxygen anion having more charge tends to be more stable).

### Experimental band gap

Fig. 6 shows the diffuse reflectance spectrum of $K_3LaTe_2O_9$. The absorption edge of $K_3LaTe_2O_9$ is 287 nm, from which a band gap of 4.32 eV is deduced.[33]

### Thermal analysis

As shown in Fig. 7(a), the TGA curve of $K_3LaTe_2O_9$ exhibits continuous weight loss during the heating process and complete decomposition at 979 °C. The DSC heating curve (Fig. 7(b)) of $K_3LaTe_2O_9$ exhibits two sharp endothermic peaks at 755 °C and 845 °C, respectively, which also indicates that it decomposes during heating. Therefore, single crystals of $K_3LaTe_2O_9$ must be grown by the flux method below the decomposition temperature.

### Variable-temperature X-ray powder diffraction (VT-XRD)

To further investigate the thermal properties of $K_3LaTe_2O_9$, variable-temperature X-ray powder diffraction was performed. As seen in Fig. 8, impurity peaks appeared when the temperature increased. The main component of the polycrystalline sample at 923 K is $K_3LaTe_2O_9$, with the impurity peaks corresponding to $La_2TeO_6$. The $K_3LaTe_2O_9$ had decomposed completely to $La_2TeO_6$ at 1023 K.

### IR and Raman spectra

Fig. 9 shows the IR spectrum in the region of 400 $cm^{-1}$ to 1200 $cm^{-1}$, and the Raman spectrum between 100 $cm^{-1}$ and 1200 $cm^{-1}$, by which it is difficult to confirm completely the coordination of Te atoms due to their complexity. It can be roughly inferred that the bands from 600 to 800 $cm^{-1}$ (729 $cm^{-1}$ and 768 $cm^{-1}$) correspond to the Te–O(2) stretching mode. Infrared vibration (565 $cm^{-1}$) observed in the

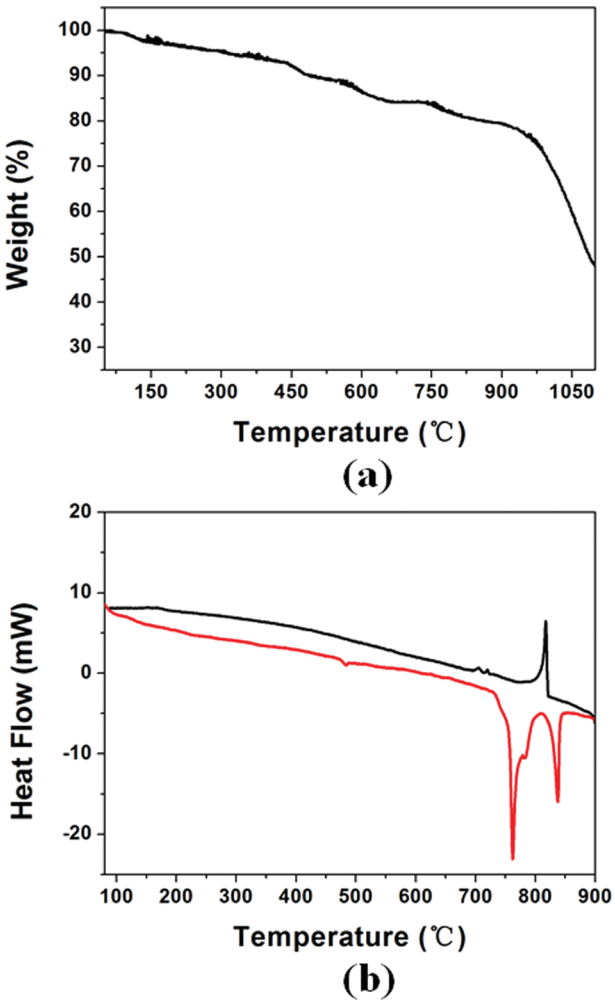


Fig. 7 TGA and DSC patterns of $K_3LaTe_2O_9$.

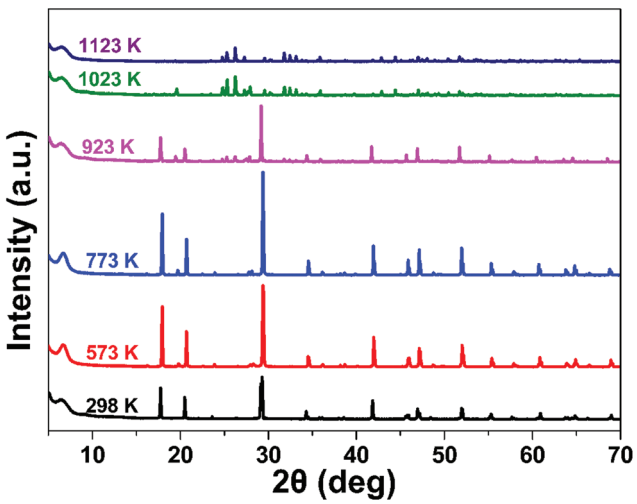


Fig. 8 Variable-temperature X-ray powder diffraction patterns from 298 K to 1123 K.

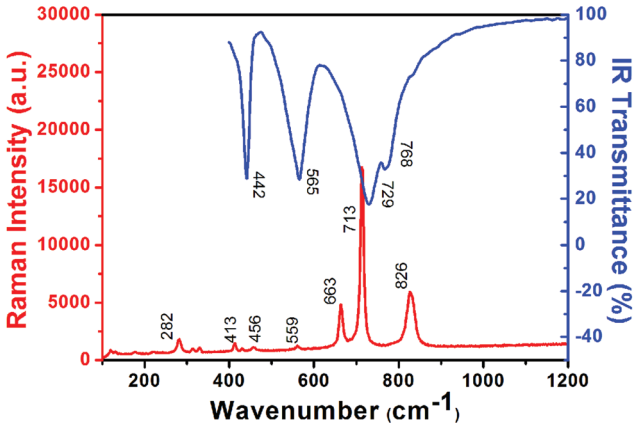


Fig. 9 Experimental IR and Raman spectra.

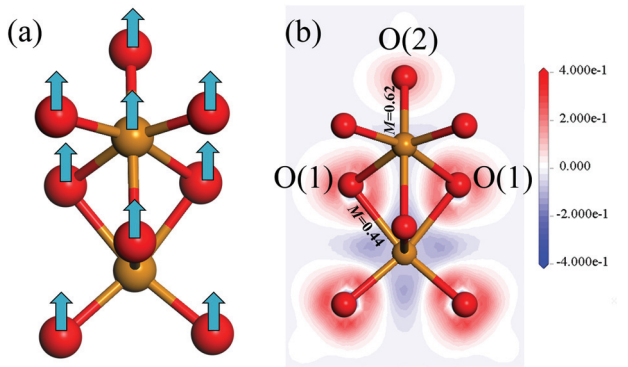


Fig. 10 (a) Vibration along the same direction of the $[Te_2O_9]$ group. (b) Contour plots of the electronic density difference on the planes formed by Te and face-sharing O. The off-plane and O atoms are represented by small red balls.

500–600 $cm^{-1}$ region is assigned to the Te–O(1) stretching mode. The bands in the low frequency region can be attributed to bending and deformation modes of the group.[12,34]

## Conclusions

A new quaternary alkali-lanthanide metal tellurate $K_3LaTe_2O_9$ has been grown as single crystals from a flux, which belongs to the hexagonal space group $P6_3/mmc$. In the structure, $[Te_2O_9]^{6-}$ contains rare face-sharing $TeO_6$ octahedra, which are connected by $LaO_6$ octahedra and form a three dimensional framework structure. The VT-XRD results and the thermal analysis show that $K_3LaTe_2O_9$ decomposes at high temperatures. The first-principles calculations demonstrate the stability of the $[Te_2O_9]$ group, while the calculated electronic density difference and Mulliken population reveal that in the $[Te_2O_9]$ group the corner-sharing oxygen atoms are more stable than the face-sharing oxygen atoms.

## Acknowledgements

This work was supported by the National Natural Science Foundation of China (Grant No. 91422303 and 11174297) and China "863" project (No. 2015AA034203).

## References

1 J. Yeon, S. H. Kim, S. D. Nguyen, H. Lee and P. S. Halasyamani, *Inorg. Chem.*, 2012, **51**, 2662.
2 R. Mathieu, S. A. Ivanov, R. Tellgren and P. Nordblad, *Phys. Rev. B: Condens. Matter*, 2011, **83**, 174420.
3 M. S. Augsburger, M. C. Viola, J. C. Pedregosa, R. E. Carbonio and J. A. Alonso, *J. Mater. Chem.*, 2006, **16**, 4235.
4 M. Sathiya, K. Ramesha, G. Rousse, D. Foix, D. Gonbeau, K. Guruprakash, A. S. Prakash, M. L. Doublete and J. M. Tarascona, *Chem. Commun.*, 2013, **49**, 11376.
5 J. Choisnet, A. Rulmont and P. Tarte, *J. Solid State Chem.*, 1989, **82**, 272.
6 V. B. Nalbandyan, M. Avdeev and M. A. Evstigneeva, *J. Solid State Chem.*, 2013, **199**, 62.
7 Y. S. Hong, M. Zakhour, M. A. Subramanian and J. Darriet, *J. Mater. Chem.*, 1998, **8**, 1889.
8 M. Liegeois-Duyckaerts, *Spectrochim. Acta, Part A*, 1985, **41**, 523.
9 W. S. Zhang and H. J. Seo, *J. Alloys Compd.*, 2013, **553**, 183.
10 M. Kunz and I. D. Brown, *J. Solid State Chem.*, 1995, **115**, 395.
11 (*a*) M. L. López, M. L. Veiga and C. Pico, *J. Mater. Chem.*, 1994, **4**, 547; (*b*) M. C. Knapp and P. M. Woodward, *J. Solid State Chem.*, 2006, **179**, 1076; (*c*) M. L. López, I. Alvarez, M. Gaitán, A. Jerez, C. Pico and M. L. Veiga, *Solid State Ionics*, 1993, **63**, 599.
12 A. J. Jacobson, J. C. Scanlon, K. R. Poeppelmeier and J. M. Longo, *Mater. Res. Bull.*, 1981, **16**, 359.
13 Rigaku, *CrystalClear*, Rigaku Corporation, Tokyo, Japan, 2008.
14 G. M. Sheldrick, *Acta Crystallogr., Sect. A: Fundam. Crystallogr.*, 2008, **64**, 112.
15 L. M. Gelato and E. Parthé, *J. Appl. Crystallogr.*, 1987, **20**, 139.
16 R. S. Mulliken, *J. Phys. Chem.*, 1955, **23**, 1833.
17 M. C. Payne, M. P. Teter, D. C. Allan, T. A. Arias and T. A. J. D. Joannopoulos, *Rev. Mod. Phys.*, 1992, **64**, 1045.
18 S. J. Clark, M. D. Segall, C. J. Pickard, P. J. Hasnip, M. J. Probert, K. Refson and M. C. Payne, *Z. Kristallogr. – Cryst. Mater.*, 2005, **220**, 567.
19 W. Kohn and L. J. Sham, *Phys. Rev.*, 1965, **140**, 1133.

20 (*a*) J. P. Perdew and A. Zunger, *Phys. Rev. B: Condens. Matter*, 1981, **23**, 5048; (*b*) D. M. Ceperley and B. J. Alder, *Phys. Rev. Lett.*, 1980, **45**, 566.
21 J. S. Lin, A. Qteish, M. C. Payne and V. Heine, *Phys. Rev. B: Condens. Matter*, 1993, **47**, 4174.
22 L. Kleinman and D. M. Bylander, *Phys. Rev. Lett.*, 1982, **48**, 1425.
23 H. J. Monkhorst and J. D. Pack, *Phys. Rev. B: Condens. Matter*, 1976, **13**, 5188.
24 W. Klein, J. Curda, E.-M. Peters and M. Jansen, *Z. Anorg. Allg. Chem.*, 2005, **631**, 2893.
25 L. Pauling, *J. Am. Chem. Soc.*, 1929, **51**, 1010.
26 J. K. Burdett and T. J. McLarnan, *Am. Mineral.*, 1984, **69**, 601.
27 C. T. Chen, T. Sasaki, R. K. Li, Y. C. Wu, Z. S. Lin, Y. Mori, Z. G. Hu, J. Y. Wang, G. Aka and M. Yoshimura, *Nonlinear Optical Borate Crystals*, Wiley-VCH, 2012.
28 (*a*) C. Meade, R. J. Hemley and H. K. Mao, *Phys. Rev. Lett.*, 1992, **63**, 1387; (*b*) M. Grimsditch, *Phys. Rev. Lett.*, 1984, **52**, 2379; (*c*) R. M. Hazen, L. W. Finger, R. J. Hemley and H. K. Mao, *Solid State Commun.*, 1989, **72**, 507.
29 (*a*) A. K. Cheetham, G. Ferey and T. Loiseau, *Angew. Chem., Int. Ed.*, 1999, **38**, 3268; (*b*) M. Estermann, L. B. Mccusker, C. Baerlocher, A. Merrouche and H. Kesler, *Nature*, 1991, **352**, 320; (*c*) P. Y. Feng, X. H. Bu, S. H. Tolbert and G. D. Stucky, *J. Am. Chem. Soc.*, 1997, **119**, 2497; (*d*) R. K. Brow, R. J. Kirkpatrick and G. L. Turner, *J. Am. Chem. Soc.*, 1993, **76**, 919.
30 (*a*) B. Stöger, M. Weil and E. Zobetz, *Z. Kristallogr. Crystalline Mater.*, 2010, **225**, 125; (*b*) P. Höss and T. Schleid, *Z. Anorg. Allg. Chem.*, 2007, **633**, 1391.
31 (*a*) H. Huppertz and B. von der Eltz, *J. Am. Chem. Soc.*, 2002, **124**, 9376; (*b*) H. Huppertz and W. Schnick, *Chem. – Eur. J.*, 1997, **3**, 249.
32 L. Yang, W. L. Fan, Y. L. Li, H. G. Sun, L. Wei, X. F. Cheng and X. Zhao, *Inorg. Chem.*, 2012, **51**, 6762.
33 O. Schevciw and W. B. White, *Mater. Res. Bull.*, 1983, **18**, 1059.
34 R. L. Frost and E. C. Keeffe, *J. Raman Spectrosc.*, 2009, **40**, 249.

 